To do:

Figure 2.11.12 of Hansen et al. has an interface height denoted by H. This should be changed to Δz_M * *to match my notation. We need to get the eps version of the file from him. Also need 2.11.11 from him.*

I have two versions of Figure 2.11.2. One shows just the density and the other shows separate density and temperature sections. The current text uses only the density section.

2.11 Anatomy of an overflow

As outlined in Introduction, there are two major overflows that supply dense water from the Nordic Seas to the Atlantic Ocean. Each flow represents a substantial source of North Atlantic Deep Water. The Denmark Strait overflow, which has already been described, is traditionally regarded as an example of a rotating, hydraulically controlled flow. Dense fluid spills over the sill and forms a descending current that is banked against the Greenland slope. Strong interactions with shallower layers are evident and these cloud comparisons with the simple models that we have explored. Some portions of the flow have been observed to be strongly barotropic, possibly due to interactions with the East Greenland Current. The latter generally lies to the east of the overflow, but also covers much of it with a layer of lighter, southward-flowing, low-salinity water. In addition, the descending outflow contains large, horizontal eddies whose expressions can be seen at the free surface. All of these factors make it difficult to think of the overflow as isolated and lying below motionless fluid.

In contrast, the deep current in the Faroese Channel system, situated between Iceland and Scotland, is more stable and less engaged with surface layers. The deep Norwegian Sea is drained to the south through the Faroe-Shetland Channel, which lies to the east of the Faroe Islands (Figure 2.11.1). After passing the Wyville-Thompson Ridge, the channel makes a sharp bend to the northwest and becomes the Faroe Bank Channel. The most constricted section occurs at 'D' where the shallowest (850m) topography and narrowest width coincide. From there the channel bottom gradually descends for 60km and then plummets into the Iceland Basin of the North Atlantic. A combination of intermediate and deep-water masses enters this system from the Norwegian Sea. A small fraction of the volume flux leaks southward across the Wyville-Thompson Ridge (Hansen and Osterhus 2000), but the bulk continues into the Faroe Bank Channel and over the sill. It then spills down to about 4000 m in the Iceland Basin.

Though not without complexity, this overflow provides one of the more clear-cut examples of a hydraulically controlled flow that is dramatically influenced by Earth's rotation. The overflow has been the subject of a number of observational programs and our treatment relies on a 2000 survey (Mauritzen et al. 2005, Girton et al. 2005). We now describe the flow in more detail, using data collected across the lettered sections indicated in Figure 2.11.1. Some of the sections were repeated in order to gain a measure of time variability.

(*a*) *Hydrographic Properties*

A longitudinal section of potential density (σ_θ) has been constructed along the axis of the deep current from the data at the individual cross sections (Figure 2.11.2). The isopycnals slopes suggest spilling of dense water as it flows from right to left out of the Norwegian Sea, over the sill (near D), and down into the Iceland Basin of the North Atlantic proper. Were the isopycnals associated with a broad-scale, nearly geostrophic flow, such as in a subtropical gyre, the along-channel isopycnal tilt would imply a 'thermal wind'; that is, a vertically, geostrophic, cross-channel velocity. The expectation here is that the cross-channel velocity is not geostrophically balanced and that the isopycnal tilt is instead due to inertial acceleration, present in the hydraulic models we have already discussed, or perhaps due to friction acting along the channel. In either case the tilt need not imply cross-channel motion. In fact, the observations indicate flow primarily along the channel axis, though actual resolution of the transverse and longitudinal components is not accomplished. Downstream of the sill, where the tilts are strongest, the dense water experiences enhanced mixing and entrainment of overlying fluid. The resulting dilution of the overflow is suggested by the reduction or disappearance of the densities greater than σ_θ=28.00.

Potential temperature can be used as a proxy for density in this overflow and many past discussions have used the temperature structure to perform geostrophic estimates of volume flux and to define a hypothetical interface. Temperature sections A, D, F, and H (Figures 2.11.3-6) contain clear evidence of rotation in the form of strong isothermal tilt across the channel. Were the upper fluid motionless, which clearly is never completely true, then a downward tilt toward the left would indicate a flow toward the Atlantic. In section A, which is 300 km upstream of the sill (at the far right in Figure 2.11.2) water colder than 4^0C occupies the upstream channel below about 400 meters except near both sides, where the isotherm tilts downward. Mauritzen et al. (2005) describe the 4^0C isotherm as defining the upper temperature limit of the dense water that ultimately descends to great depths in the North Atlantic. (Some investigators use the 3^0C surface as a boundary for calculating volume transport.) The tilt along the left side nominally indicates a current along the left side of the channel directed toward the sill, and thus toward the North Atlantic. The tilt along the right side appears to indicate a current directed away from the sill (toward the Norwegian Sea). Whether the implied countercurrent is a robust feature is not known. The two other isothermal surfaces (7.5 and 0.5^0C) also tilt downward in the same way on the left, and the 0.5^0C surface does so on the right. This suggests that many layers within the deeper fluid act with some coherence.

It has become traditional to think of overflows as being separated into two regions with distinct dynamics. The first begins at the upstream end of the channel, here the entrance into the Faroe-Shetland Channel, and ends at the sill (section D). The flow between these two sections is often thought of as inviscid and conservative. The second portion extends downstream from the sill and contains the descending 'outflow' or

plume, often marked by enhanced turbulence, mixing, spreading, and entrainment of overlying fluid. The controlling dynamics is strongly non-conservative and is often dominated by a balance between bottom drag, entrainment stresses, gravity, and rotation. Mauritzen et al. (2005) has calculated stresses in the water column in order to identify regions of enhanced mixing and drag. Although both processes are enhanced in the Faroe-Bank plume region, they are not necessary negligible in the approach region and may, in fact, be large enough to significantly modify momentum and energy budgets. The dichotomy between an inviscid upstream region and a dissipative plume is therefore not as clear-cut as traditionally assumed.

The development of the descending plume is illustrated in temperature Sections D-H (figures 2.11.4-6). The sill section (D) is also the narrowest and the isothermal tilt there suggests a unidirectional flow of water toward the Atlantic below 4°C. Section E is slightly deeper, much wider, and lies where the along-axis slope suddenly become much steeper. The current itself is wider there and still unidirectional. At section H furthest downstream the current has spread to an even greater width and continues to be unidirectional. The water in the layer is noticeably warmer; for example there is only a small portion colder than $0.5\ ^0C$. A broader view showing both the upstream region and descending plume is given by the complete suite of sections (Figure 2.11.7). The panels, which proceed downstream from top to bottom, show the σ_θ=27.65 isopycnal, sometimes used to represent a hypothetical interface. The spreading of the outflow and its confinement to the right bank of the descending channel is evident. Multiple realizations of the interface corresponding to repeat measurements indicate a significant amount of time variability.

(*b*) *Geostrophic and direct velocity.*

It can be useful for readers unfamiliar with physical oceanography to perform the simple exercise of estimating velocity of the flow using a geostrophic balance. We now do so at section D, leaving the remaining sections as homework exercises. Begin by thinking of the entire overflow as being contained in a single layer, with the 7.5^0C isotherm representing the bounding interface. The density data in Figure 2.11.2 can be used to estimate the difference between the average density of the deep layer and that of the overlying fluid. The resulting relative change $\Delta\rho/\rho_o$ is approximately $5\text{x}10^{-4}$. Using temperature as a proxy for density, the isopycnals corresponding to the 7.5^0C isotherm has a δ=200m meters descent over a width of W=20km kilometers. With typical value of the Coriolis parameter rounded off to $f = 10^{-4}$ s $^{-1}$, the geostrophic velocity is

$$v = \frac{g\Delta\rho\delta}{\rho f W}, \qquad (2.11.1)$$

or 0.67 m s^{-1}. The depth of the layer is about D=400 m on average, which leads to a volume flux estimate of 4.0 Sv. for water colder than 7.5^0C. The flux of water colder than 4^0C, which was mentioned above to define the water reaching great depth in the Atlantic, could be estimated to be about half that number.

Overall, geostrophic estimates of velocity using the simple method described above range from 0.1 to 0.67 m s^{-1}. These values are somewhat smaller than those directly measured with a lowered profiling current meter (Figure 2.11.8a). At locations B and C upstream of the sill, the greatest current meter speed is about 0.4 meters per second, whereas the most constricted section (D) has speeds approaching 1 m s^{-1}. In these three locations there is a surface current in the opposite direction and with speeds that can approach those of the deep flow. It is not clear that interactions with this shallow flow are negligible. The deep velocities at E-H are considerably larger than those of the overlying fluid. Speeds vary, with maximum values at F, G and H of 0.9 m s^{-1}, 1.1 m s^{-1} and 0.5 m s^{-1} respectively. These sections also show how the deep current thins in the downstream direction.

The velocity measurements can be averaged over the depth of the dense outflow to produce a single-layer representation (Figure 2.11.8b). The plan view also gives the layer thickness over which the averaging was done and the value of the Froude number (discussed below) based on that thickness and average velocity. There is an indications of reverse flow along the edges of the current upstream of the sill. In the downstream plume region, the thickest, highest-speed portion of the flow lies one its deepest (left) side. Over shallower regions of the slope, the velocities are smaller and less coherent.

Because density and velocity profiles were measured across each section, one can make a comparison between the measured speeds and geostrophic estimates. The geostrophic velocity at the middle of Section D is plotted along with the average of the two accompanying direct velocity profiles (Figure 2.11.9). The direct profiles contain more fine structure than the geostrophic profile, an artifact of smoothing of the temperature and salinity data. In addition, the direct velocity profiles show a bottom boundary layer. The geostrophic profile, which does not account for frictional effects, has no such feature.

(*c*) *Volume Flux*

Volume flux estimates made using the direct velocity data show variability from section to section (Figure 2.11.10), but with a general increase in flux downstream of the sill. Repeat sections, usually taken a few weeks apart, indicate considerable time variability as well, perhaps from the natural variability of the current itself, or from eddies, tides, or surface forcing. The estimate of flux for the deep overflow water are all positive, indicating a flow from the Greenland-Norwegian Sea toward the Atlantic. There is one very large, and unexplained, estimate at section A. One possibility is that this estimate is correct, but there that is loss of water in the upstream channel from a flux of deep water over the Wyville-Thompson ridge, as mentioned earlier. The overall increase in transport from Section D to H is thought to be due to the turbulent entrainment of overlying warmer water into the deep current. This view is supported by the observation that the overflow becomes warmer and less dense as it descends.

Sill flow toward the North Atlantic has been found every time measurements have been made. For example, Borenas and Lundberg (1988) estimated a geostrophic transport of 1.8 Sv below 3^0C with data collected in 1983. Although this value is in good agreement with present data, no clear picture of time-dependence was acquired. To detect changes in the flow over a few months duration, Saunders (1990) deployed an array of current meters in the passage in 1987 and recovered them in 1988. Although many of the current meters were lost, velocity records of the cold overflow water with 363 days duration at depths of 492 and 693 m were recovered from one mooring. The current was found to persist all year with only a small seasonal fluctuation. The average volume flux of water colder than 3.0 degrees C was estimated to be 1.9 Sv, which is quite close to the other estimates.

More recent measurements of longer duration indicate a stronger seasonal variation along with a long-term trend. The current at the sill has been measured with upward looking profiling acoustic Doppler current profilers (ADCPs) since 1995. The corresponding transports (Figure 2.11.11) suggests a seasonal cycle below 3^0C with maximum outflow during the spring. Hansen et al. (2001) used the same data to calibrate a relation between the transport and the upstream elevation Δz_M * above the sill of the $\sigma_t = 28.0$ surface. This elevation can be found from hydrographic data monitored by Ocean Weather Ship-M, positioned in the eastern Norwegian Sea about 400 km upstream of the sill. The *ad hoc* relationship resembles a weir relation, with transport proportional to a power of Δz_M *. A comparison between the calibrated relation and the measured transport appears in the figure. The weather ship has produced a temperature and salinity data set in the Norwegian Sea since 1948 and a time history of the depth of $\sigma_t = 28.0$ can be extracted from this record. This history was used by Hansen et al. (2001) in conjunction with the calibrated transport relation to estimate a history of transport over the period 1950-2000 (Figure 2.11.12). The value of Δz_M * has diminished over this period and the corresponding decrease in transport is estimated to be about 20%. Continuation of such a trend would have important consequences for the meridional overturning cell in the Atlantic Ocean and therefore for climate. Some caution should be used in interpretating this result; for one thing, the Gill (1977) model calls into question the idea that transport can be monitored using a single upstream measurement. This and set of related questions are taken up in Section 2.14.

(*d*) *Potential Vorticity*

One of the key assumptions of the benchmark hydraulic models is that of uniform potential vorticity. Lake et al. (2005) estimated potential vorticity using three acoustic current profilers deployed across the sill for 69 days. The relative vorticity is estimated using differences in velocities between neighboring profiles, while the interface position is estimated from the vertical shear. The result is are two side-by-side potential vorticity time series. The contribution of the lateral shear was found to be roughly 1/4 as large as Coriolis parameter f. In addition the shear was negative, a result consistent with the layer being thinner at the sill than upstream. The magnitude of the potential vorticity varied by a factor of two during the measurements. The average values of the two side-

by-side locations differed by about 30%. Therefore, the assumption of constant potential vorticity is not obeyed in detail. It varies in space and time but may still be a useful first approximation.

(*e*) *Hydraulic Criticality*

The Faroe-Bank Channel inspired the Borenäs and Lundberg's (1986) theory of uniform potential vorticity flow in a parabolic channel, discussed in Section 2.8. The authors follow this work with a (1988) report on the first large-scale observational study of the overflow. Among other findings, their critical condition appears to be satisfied, or nearly so, at the sill. Model estimates of volume flow range from 1.5 to 2.5 Sv., which compare well with their measured 1.5 to 1.9 Sv. By contrast, zero potential vorticity estimates for flow through a passage with a rectangular cross section give 2.1 to 3.4

Girton et al. (2006) report on an expanded effort to verify that the Faroe-Bank Channel flow becomes hydraulically critical and to determine the position of the critical section. The authors compute three independent indicators of flow criticality, the most general and reliable of which is the phase speed of the long-wave modes of the flow. The speeds are found by treating the observed flow at each section as a basic, steady parallel state and calculating the linear normal modes of this state. An approximation of the actual bottom topography at the sections in question is used. In each case two Kelvin-like modes are found, one trapped to the right wall and one to the left wall (Figure 2.11.13). These modes are similar to what would be found in a model with uniform potential vorticity. However, the non-uniformity of the actual potential vorticity gives rise to a class of potential vorticity modes. A section-by-section compilation (Figure 2.11.14) shows that the phase speeds of the potential vorticity modes (dashed lines) are bounded by the Kelvin wave speeds (solid lines). The right-wall Kelvin mode (upper solid line) always propagates in the downstream (positive) direction, as expected. The left-wall Kelvin model (lower solid line) has a speed that is generally upstream (negative) indicating subcritical conditions with respect that that mode. However there is a single section (F), approximately 60 km downstream of the sill, where the wave speed goes to zero, or nearly so, and this is a suggestion of critical flow in the vicinity. Note that F lies where the bottom slope increases abruptly. The sill flow itself appears by this measure substantially subcritical, which contradicts earlier work. The placement of the critical section on the downstream slope would be consistent with remarks made in the first chapter concerning the effects of friction and entrainment, though a model that includes these and retains rotation has not been developed.

Although the real part of the phase speeds associated with the potential vorticity modes are generally positive (downstream), there is a case in which one of the speeds goes to zero (lowest dashed curve). The 'critical' section in question lies at B, approximately 140km upstream of the sill. The ramifications and importance of a potential wave vorticity control are not well understood, but the topic is revisited in Chapter 6. The present situation is further complicated by the fact that some of the modes have complex phases speeds (open circles), indicating instability, in certain regions. However, since overflows are driven by gravity, the Kelvin wave control would seem to

be most relevant. As is generally the case, and suggested by the eigenfunction structures (Figure 2.11.12) the potential vorticity modes are manifested mainly in the lateral structure and horizontal velocity, and less in the elevation of the interface.

The suggestion that the Kelvin wave critical section lies downstream of the sill is generally consistent with two other measures calculated by Girton et al. (2006). One involves the parabolic Froude number for uniform potential vorticity (eq. 2.8.13). The other is the distribution of the 'local' Froude number $v/(g'd)^{1/2}$ across each section. One must exercise caution in interpreting the value of this quantity at any particular point: hydraulic criticality implies the arrest of a Kelvin mode, or some other discrete cross-channel mode. The required conditions depend on the structure of the flow across the whole cross section and not at a just single point. Nevertheless the individual values of $v/(g'd)^{1/2}$ across a particular section may give some information as to whether critical flow is *possible*. There are two guiding pieces of information: First, a local region of flow over which $v/(g'd)^{1/2}>1$ is one in which localized disturbances propagate downstream (see Appendix C or Section 4.3). Although hydraulics is more concerned with the propagation of cross-channel modes (that feel the side walls through satisfaction of boundary condition), it is clear that a section of flow having $v/(g'd)^{1/2}>1$ all the way across must be supercritical. The second piece of information concerns a conjecture that $v/(g'd)^{1/2}$ must equal one at some point across a section in order for that flow to be critical with respect to a normal mode. This result can be shown to hold for the simplified model flows that have been discussed thus far and, for example, is particularly clear in the formulation of Stern's critical condition (2.9.6). The latter holds for flow with arbitrary potential vorticity in a channel with a rectangular cross section and with unidirectional flow. The result has not been proven for cases in which the cross-section is nonrectangular or when velocity reversals exist.

A compilation of local Froude numbers at all points of direct velocity measurement indicates that values exceed unity at only two sections, G and F (Figure 2.11.15). [The quantity plotted is actually a version of $v/(g'd)^{1/2}$ adjusted to compensate for the effects of vertical shear and continuous stratification.] It is at one of these sections that the left wall Kelvin wave speed comes close to zero. There is no section over which the local Froude number that is uniformly greater than zero. In fact, one of the striking aspects of the study is the lack of evidence at any section for a strongly supercritical flow.

(*f*) *Other Reading*

A number of observational or data analysis projects have been completed as this book was being prepared. Duncan, Bryden and Cunningham (2003) used three sections of velocity and density data at the sill and up to 60 km downstream. These data, taken over a five-day span, allowed estimates of frictional and mixing rates. Results include values of the bottom drag coefficient, the Von Karmen constant of the turbulence, the turbulent diffusivity, Richardson numbers and local Froude numbers. They found that the strongest mixing, characterized by turbulent diffusivities up to $500\ \mathrm{cm^2\ s^{-1}}$, is found 20 km downstream of the sill where Richardson numbers are small. At 60 km

downstream, the diffusivities have decreased to $50\ \mathrm{cm^2\ s^{-1}}$, and Richardson numbers are generally larger.

Readers who desire to learn more about the history of observations and models of the Faroese Channel system are referred to a review by Borenäs and Lundberg (2004). In addition, a presentation created by James F. Price containing many results of the Faroe Bank Channel Field Program is available at http://www.whoi.edu/science/PO/people/jprice/website/projects_overflows.html.

Exercises

Exercise 1. Estimate geostrophic velocity, layer depth, and volume flux at sections A, F, and H using the grey lines to represent the bounding interface, bottom and sides as shown in Figure 2.11.16. Note that Section A has left and right regions that are treated separately. You can use the estimates f=10^{-4}/s and $\Delta\rho/\rho$=5x$10^{-4.}$

Our estimates are as follows:

Section A (on the left): $\delta = 100$ m, $W = 20$ km, $v = 0.25$ D=400m $\mathrm{s^{-1}}$, $Q = 2.0$. On the right: $\delta = -100$ m, $W = 15$ km, $v = 0.34$ m $\mathrm{s^{-1}}$, D=300m, $Q = -1.5$ Sv.

Section F: $\delta = 350$ m, $W = 45$ km, $v = 0.39$ m $\mathrm{s^{-1}}$, D=200m, $Q = 3.5$ Sv.

Section H: $\delta = 600$ m, $W = 110$ km, and $v = 0.27$ m $\mathrm{s^{-1}}$. We picked D=400m on the left, D=200m on the right for the average D=300m, so $Q = 8.1$ Sv.

Figure Captions

Figure 2.11.1. Bathymetric map of the Faroese Islands. The letters A-H indicate sections at which data was collected (Mauritzen, et al. 2005). An open circle marks the center of mass anomaly of the dense overflow at the time the section was taken. Multiple circles on the same section indicate repeat measurements. The upper right inset shows a density profile (dark curve) of the background Atlantic Water along with dots indicating the mean overflow density for sections D-H. *Need to know what the light grey curve is.* The path of the deepest part of the main channel system (the thalweg) is indicated by a doted line. The bathymetry is based on Smith and Sandwell (1997). (From Girton et al. 2006).

Figure 2.11.2. (a): An along-channel density (σ_θ) section based on the earliest sampling of data from Sections A-H. The section track is shown in Figure 2.11.1. The bathymetry along the thalweg is shaded gray while the bathymetry along the section track is shaded white. (From Girton et al. 2006). (b): Similar to (a) but showing the 7.5, 4.0, and 0.5 degree potential temperature contours (J. Price, private communication).

Figure 2.11.3. Potential temperature across Section "A" of Figure 2.11.1. The dashed lines reflect isotherm slope approximations used for geostrophic velocity estimates. (From J. Price, private communication)

Figure 2.11.4. Potential temperature across Section "D", which lies close to the sill and the narrowest section. (From J. Price, private communication)

Figure 2.11.5. Potential temperature across Section "F". (From J. Price, private communication)

Figure 2.11.6. Potential temperature across Section "H" downstream of the sill, where the deep water has descended a few hundred meters. . (From J. Price, private communication)

Figure 2.11.7 Stacked cross-sections. The bathymetry (thick black lines) and the σ_θ=27.65 isopycnal (thin black lines) across sections A-H. Multiple realizations of the isopycnal indicate repeat sections.

Figure 2.11.8. (a) Direct velocity measurements along the sections shown in Figure 2.11.1 and at 20m depth intervals. (From J. Price, private communication). (b) The depth-average velocity below the σ_θ=27.65 isopycnal. The circle size indicates the thickness of the deep layer and the shading indicates the magnitude of the local Froude number. The data includes repeat sections.

Figure 2.11.9. ADCP velocity data (dashed profiles) from two adjacent locations on Section D, their average (thin line), and a geostrophic velocity profile from CTD data in the two locations (thick line).

Figure 2.11.10. Volume flux estimates along the track shown by letters in Figure 2.11.2. Duplicate estimates at the same passage locations are from data taken at different times. The upper panel (a) is an estimate of volume flux alone while the lower panel (b) is an estimate for temperature-weighted volume flux. (From J. Price, private communication)

Figure 2.11.11. Estimated flux of overflow water colder than $0.3^0 C$ through the Faroe Bank Channel from mid-1995 to late in 2000. The wide line is based on current meter data. The width indicates estimated error from uncertainties in depth of the $0.3^0 C$ isotherm. The other line uses an empirical formula and data from Ocean Weather Ship-M to estimate flux. An eight month time lag gives the best coherence with the current meter data; the result from the empirical formula has been displaced that much. (From Hansen et al. 2001)

Figure 2.11.12. Depth of the density $\sigma_t = 28.0$ at Ocean Weather Ship-M from 1949 to 1999. The dots are a monthly average and the line is a five-year running mean. This data was used to infer t a 20% decrease in flux over the 50-year interval. (From Hansen et al. 2001)

Figure 2.11.13 The linear eigenfunction structures for four of the lowest modes at Section D. Black lines and symbols indicate the interface of the observed 'background' flow. The solid gray line shows the change in the interface due to the presence of the mode. The magnitude (and sign) of this change is arbitrary and has been selected for visual convenience. The difference between the vertical solid and gray lines indicates the sideway excursions of the dense water due to the presence of the mode. Modes 1 and 2 resemble Kelvin waves, whereas 4 and 8 resemble potential vorticity waves. The phase speeds are given in *m*/*s*. (From Girton et al. 2006)

Figure 2.11.14 Phase speeds for the first eight long-wave channel modes of the flow, calculated at various sections. Curves indicate averages of values calculated for repeat sections, whereas dots indicate values for specific measurements. The upper curve gives the speed of a Kelvin wave propagating along the right edge (facing downstream) of the current. The lower curve gives the speed of the left-wall Kelvin wave. The intermediate curves correspond to potential vorticity modes. Open circles indicate that the phase speed was complex, though only the real part is plotted. Positive values indicate downstream propagation. (From Girton et al. 2006)

Figure 2.11.15 Local Froude numbers measured at various points across the various sections. A correction factor α/β has been applied to attempt to correct for the effects of vertical shear and continuous stratification (see Nielsen, et al. 2004). (The uncorrected values, which are smaller, are shown in Figure 2.11.8b). The shading in the circle and the ciricle size indicates the relative size of the transport velocity *vd* at the point at which the Froude number was measured. (From Girton et al. 2006).

Figure 2.11.16 Sections A, F and H for use in homework exercise (based on J. Price, personal communication).

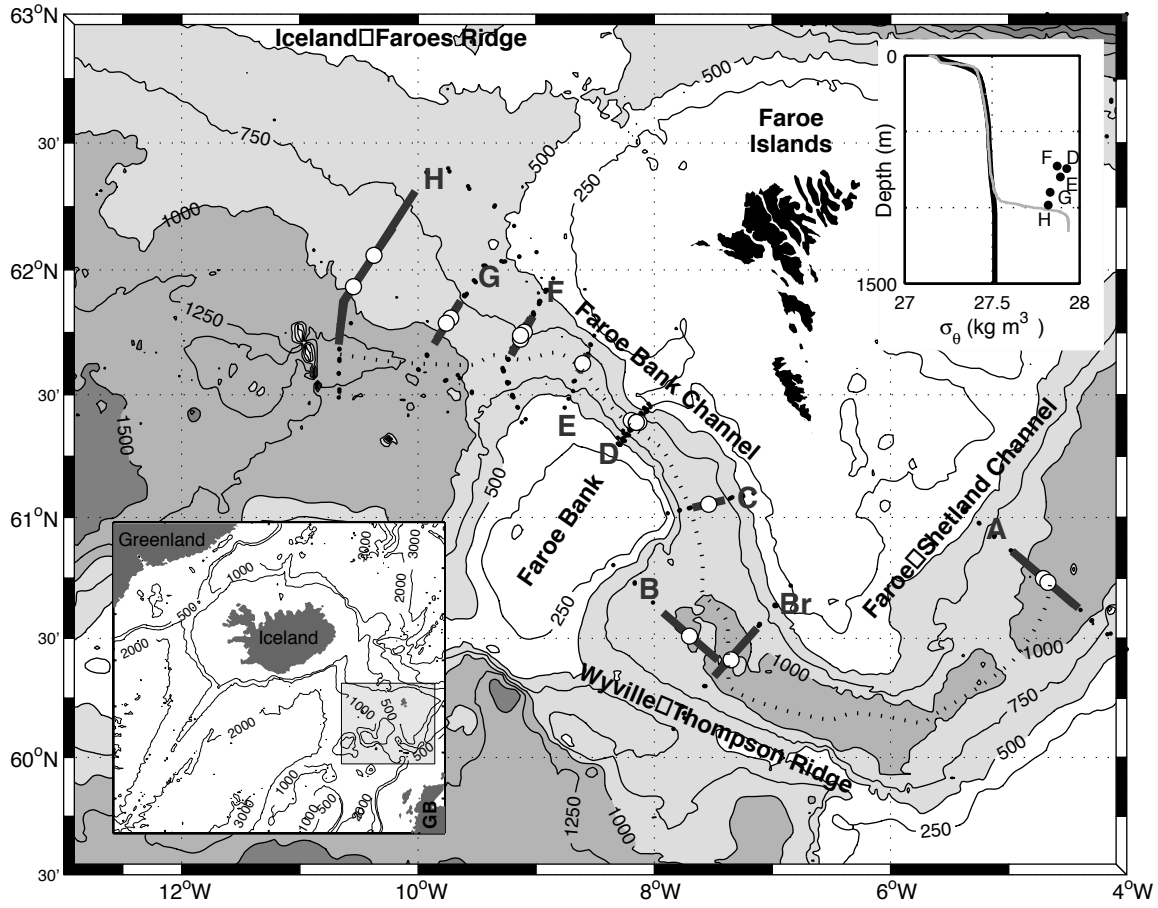
Iceland–Faroes Ridge
Faroe Islands
Faroe Bank Channel
Faroe Bank
Faroe–Shetland Channel
Wyville–Thompson Ridge
Greenland
Iceland
GB
Depth (m)
σθ (kg m3)
63°N
62°N
61°N
60°N
30'
12°W
10°W
8°W
6°W
4°W

Figure 2.11.1

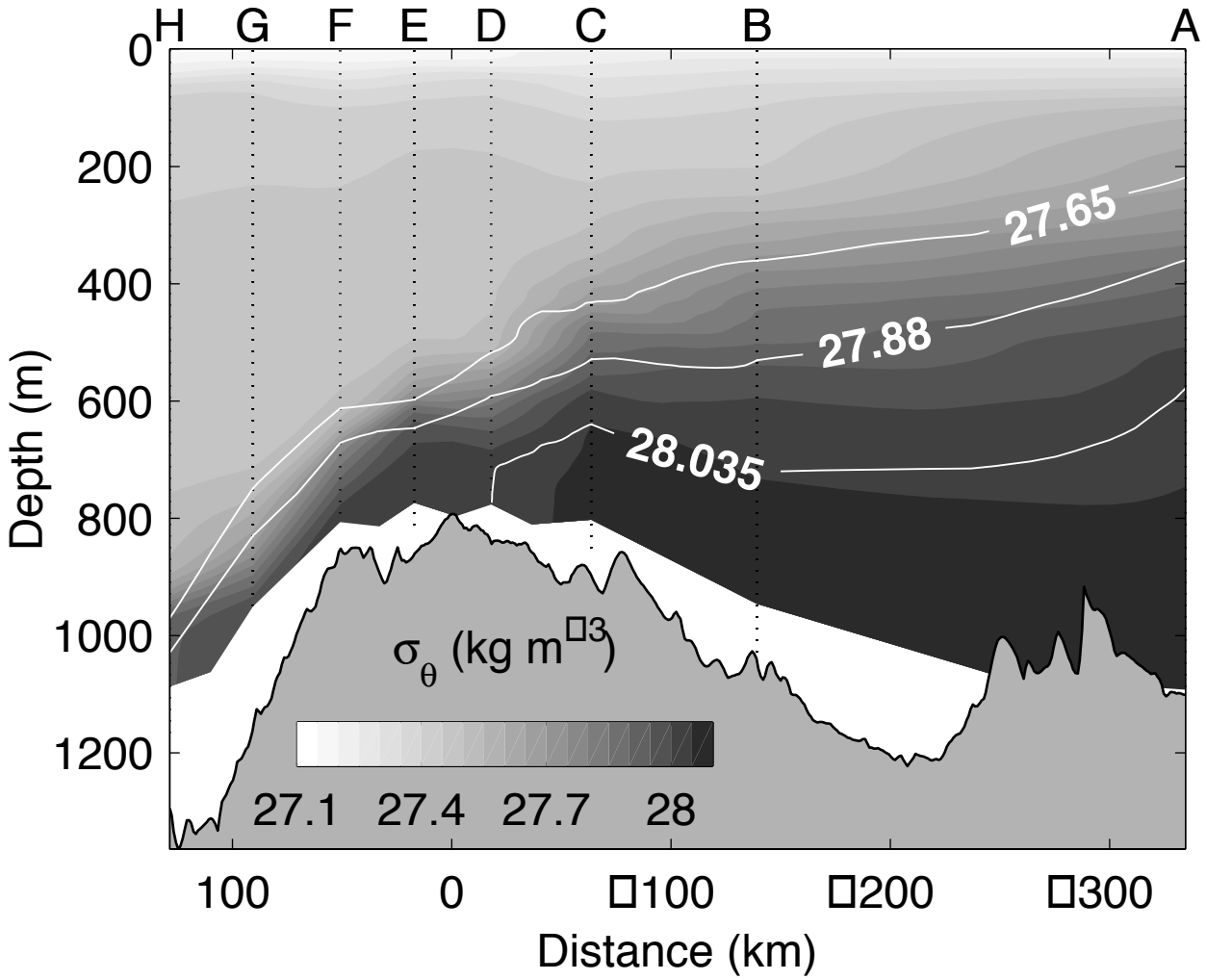
H
G
F
E
D
C
B
A
0
200
400
600
800
1000
1200
Depth (m)
27.65
27.88
28.035
σθ (kg m□3)
27.1
27.4
27.7
28
100
0
□100
□200
□300
Distance (km)

Figure 2.11.2

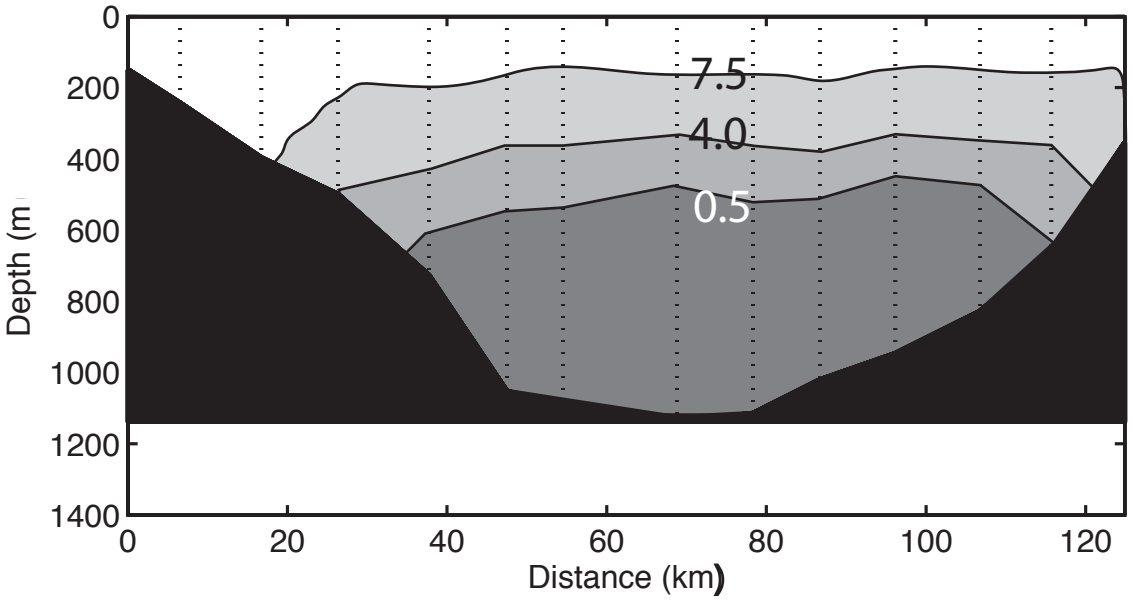
0
200
400
600
800
1000
1200
1400
Depth (m
7.5
4.0
0.5
0
20
40
60
80
100
120
Distance (km)

Figure2.11.3

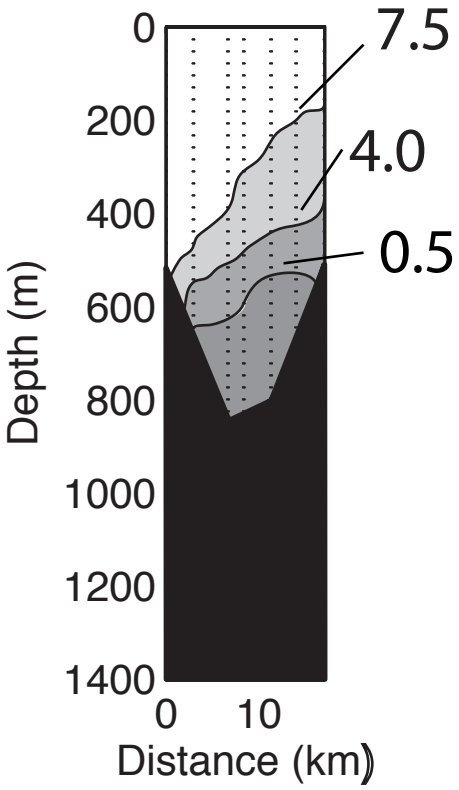
0
200
400
600
800
1000
1200
1400
Depth (m)
0
10
Distance (km)
7.5
4.0
0.5

Figure 2.11.4

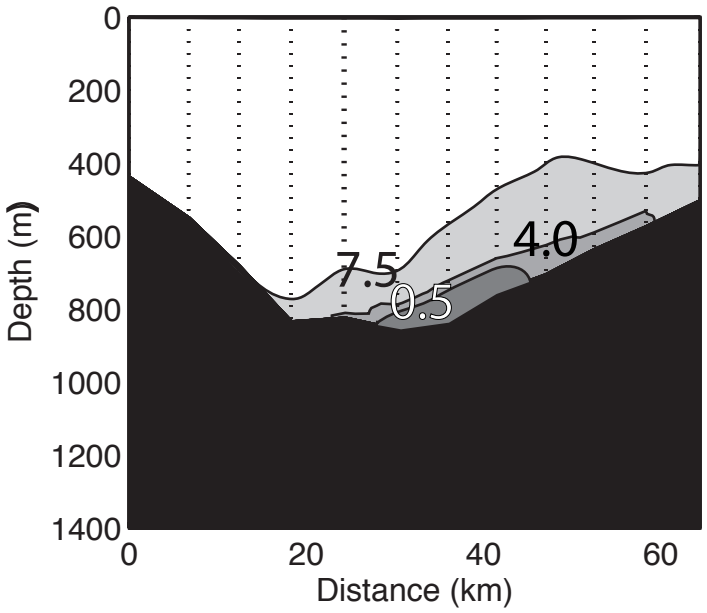
0
200
400
600
800
1000
1200
1400
Depth (m)
0
20
40
60
Distance (km)
7.5
4.0
0.5

Figure 2.11.5

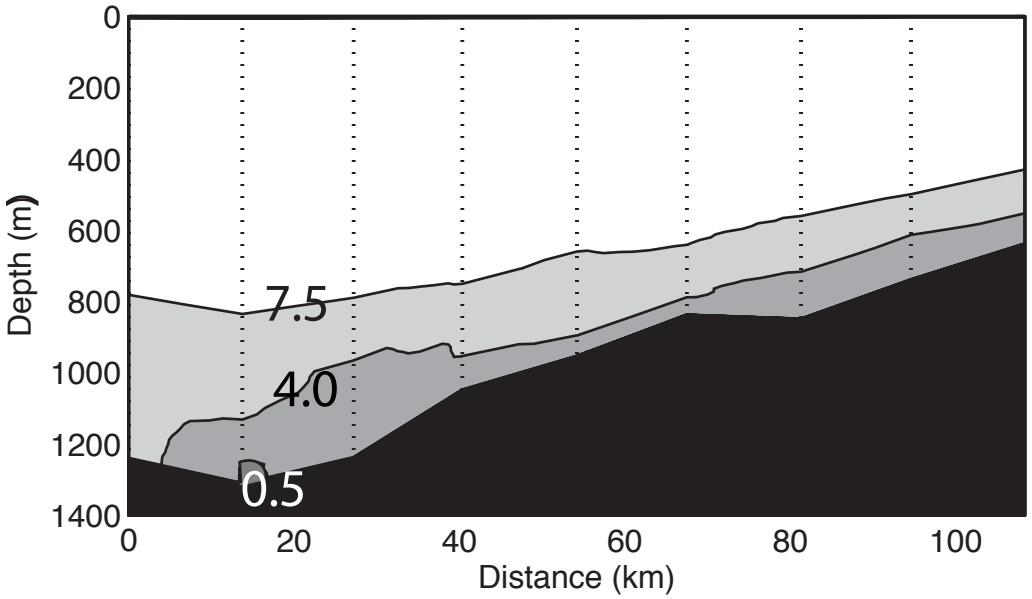
0
200
400
600
800
1000
1200
1400
Depth (m)
7.5
4.0
0.5
0
20
40
60
80
100
Distance (km)

Figure 2.11.6

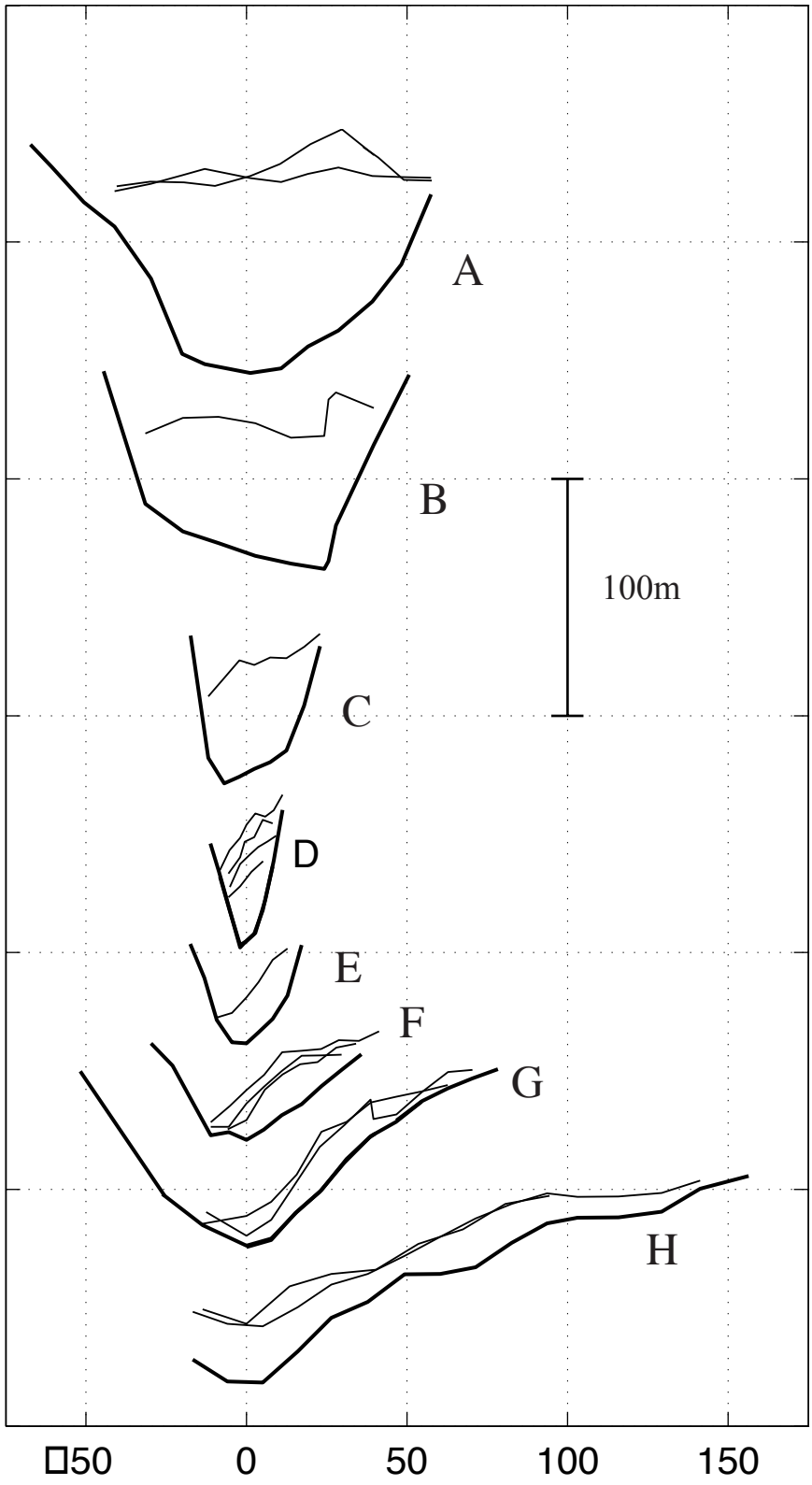

Figure 2.11.7

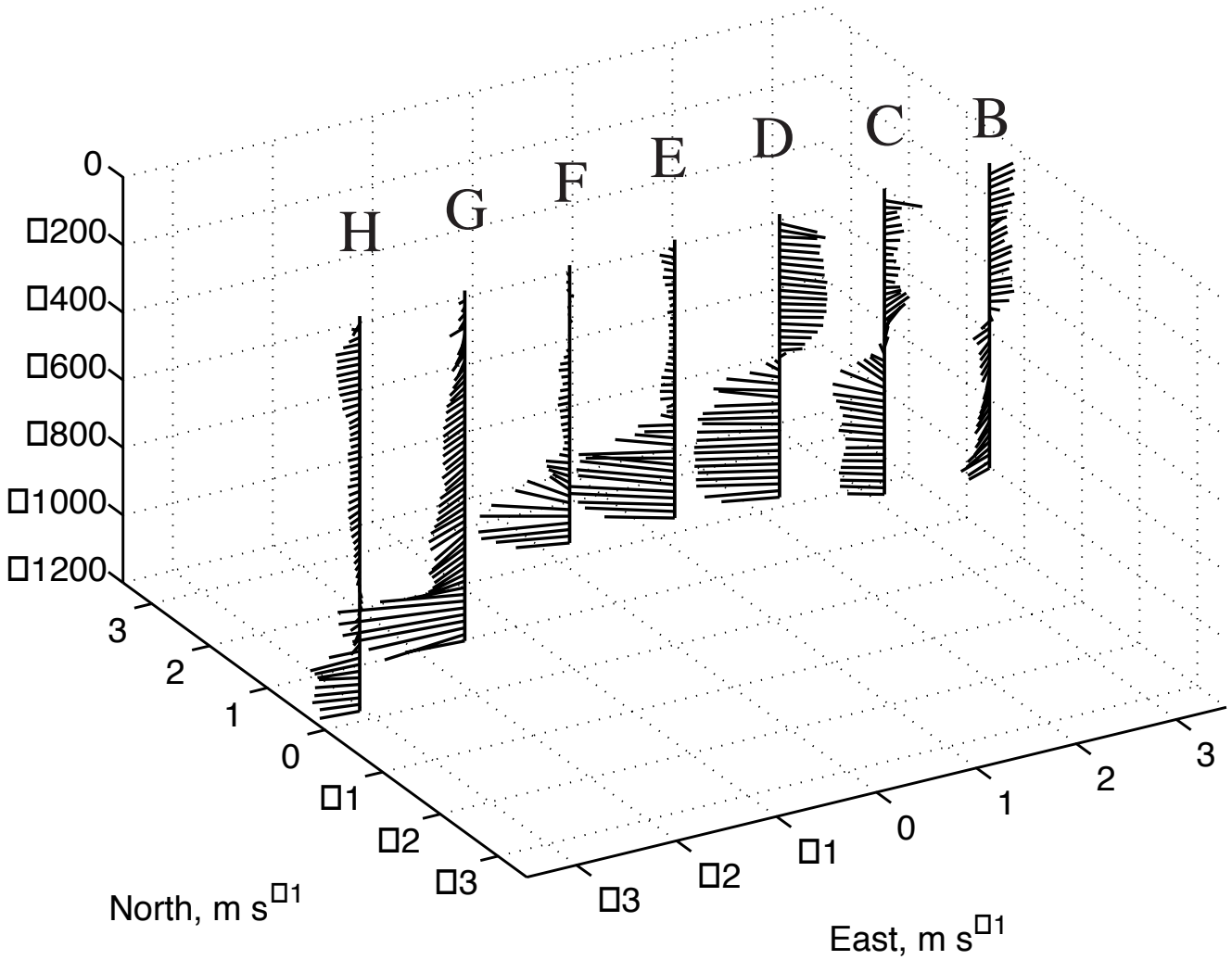

Figure 2.11.8a

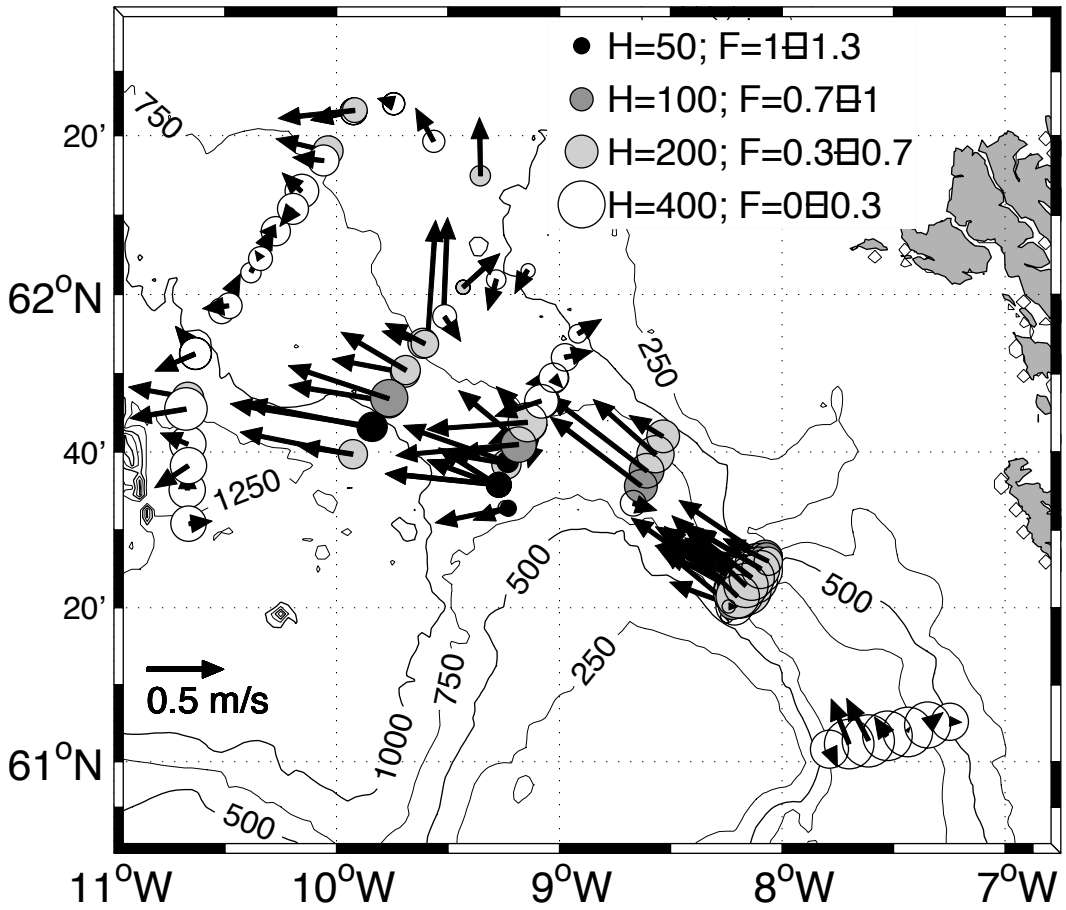

Figure 2.11.8b

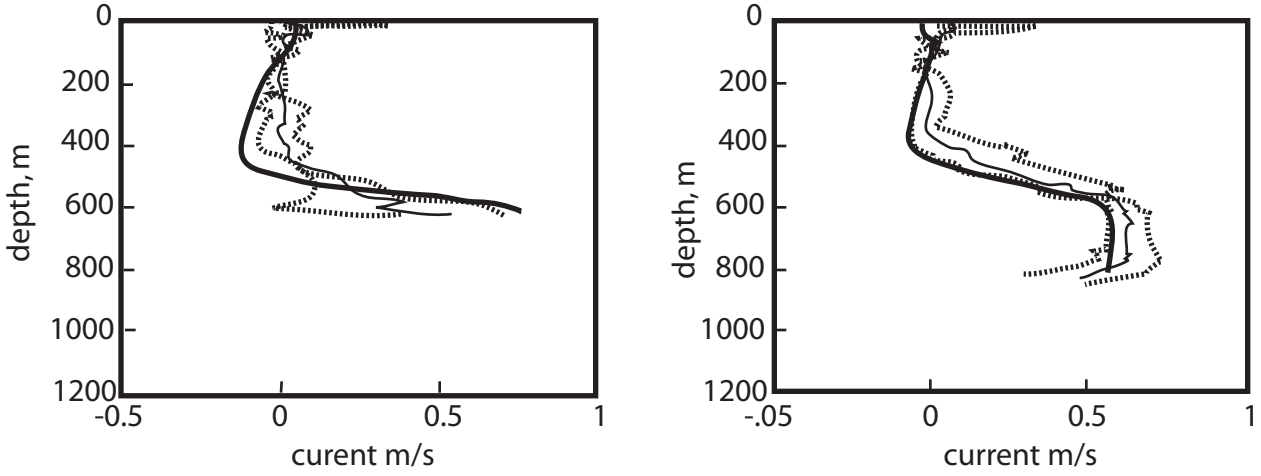
0
200
400
600
800
1000
1200
depth, m
-0.5
0
0.5
1
curent m/s
0
200
400
600
800
1000
1200
depth, m
-.05
0
0.5
1
current m/s

Figure 2.11.9

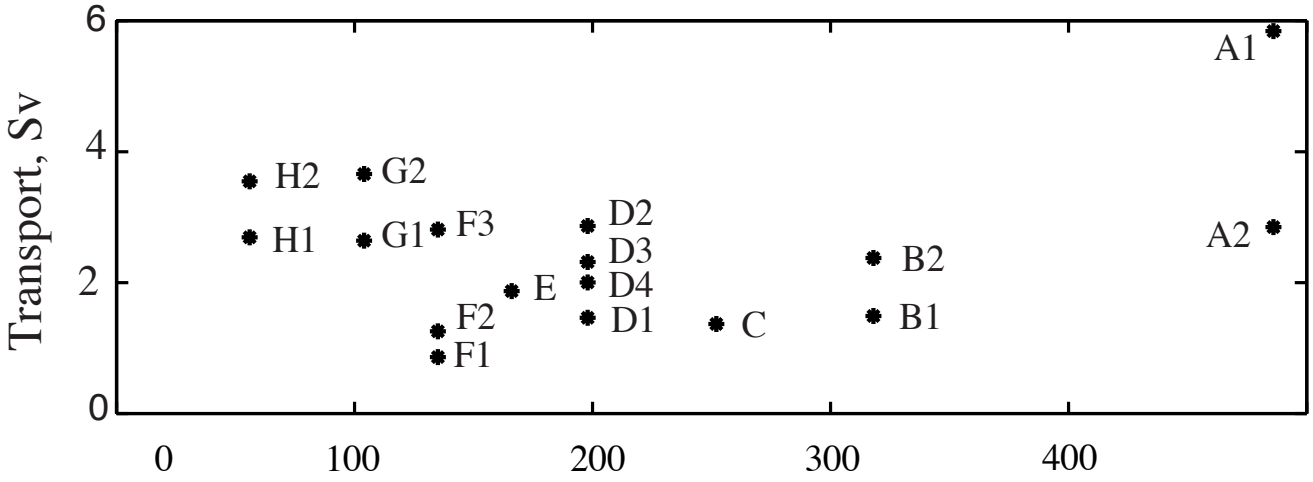

Figure 2.11.10

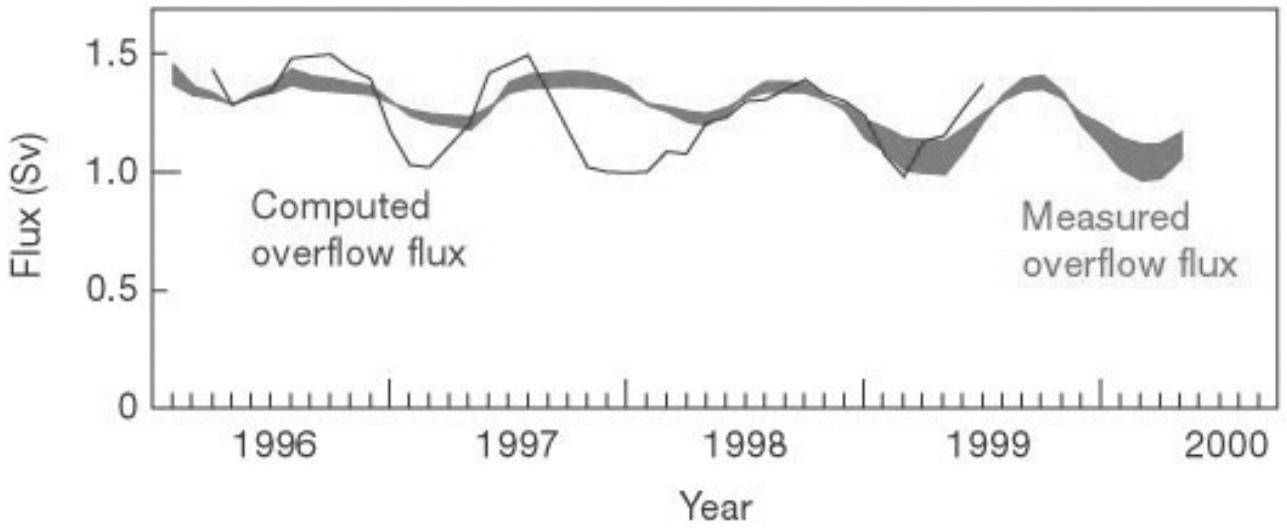

Figure 2.11.11

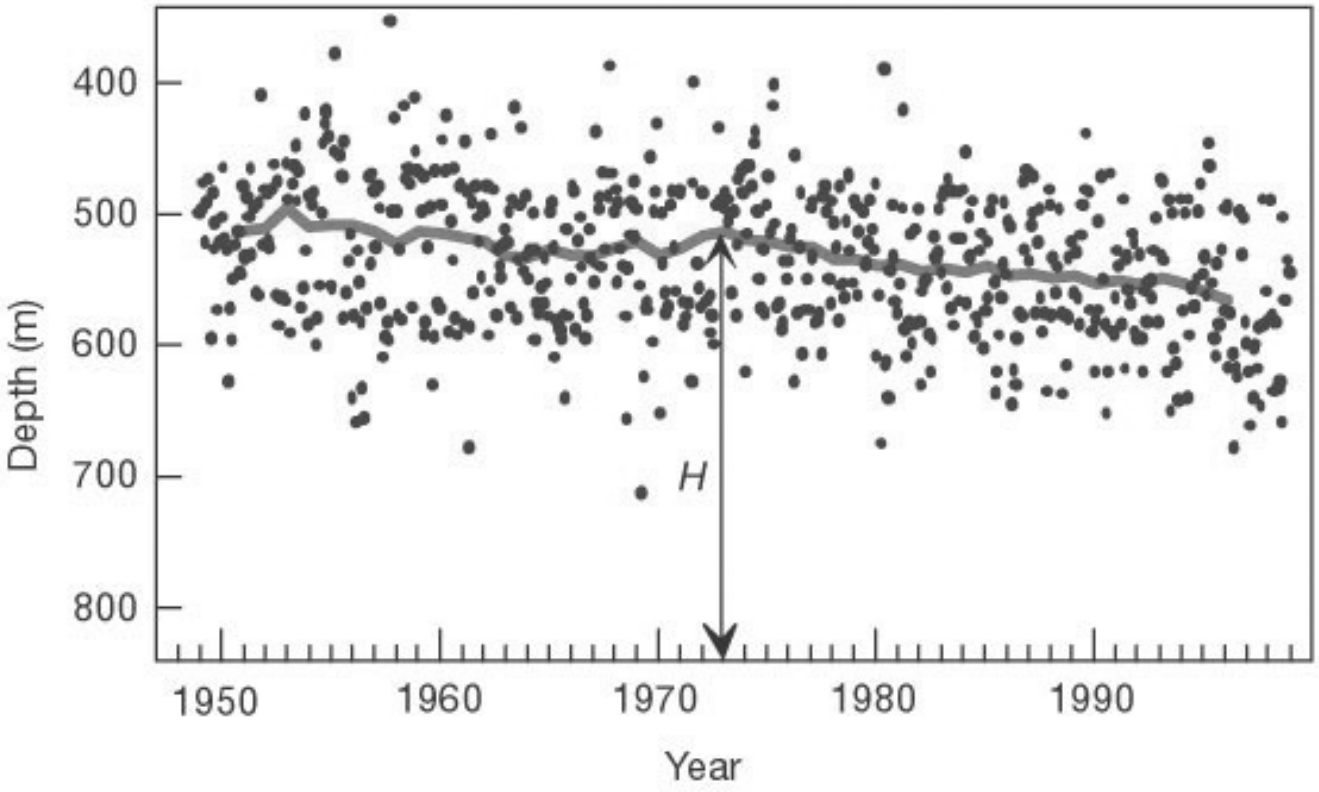

Figure 2.11.12

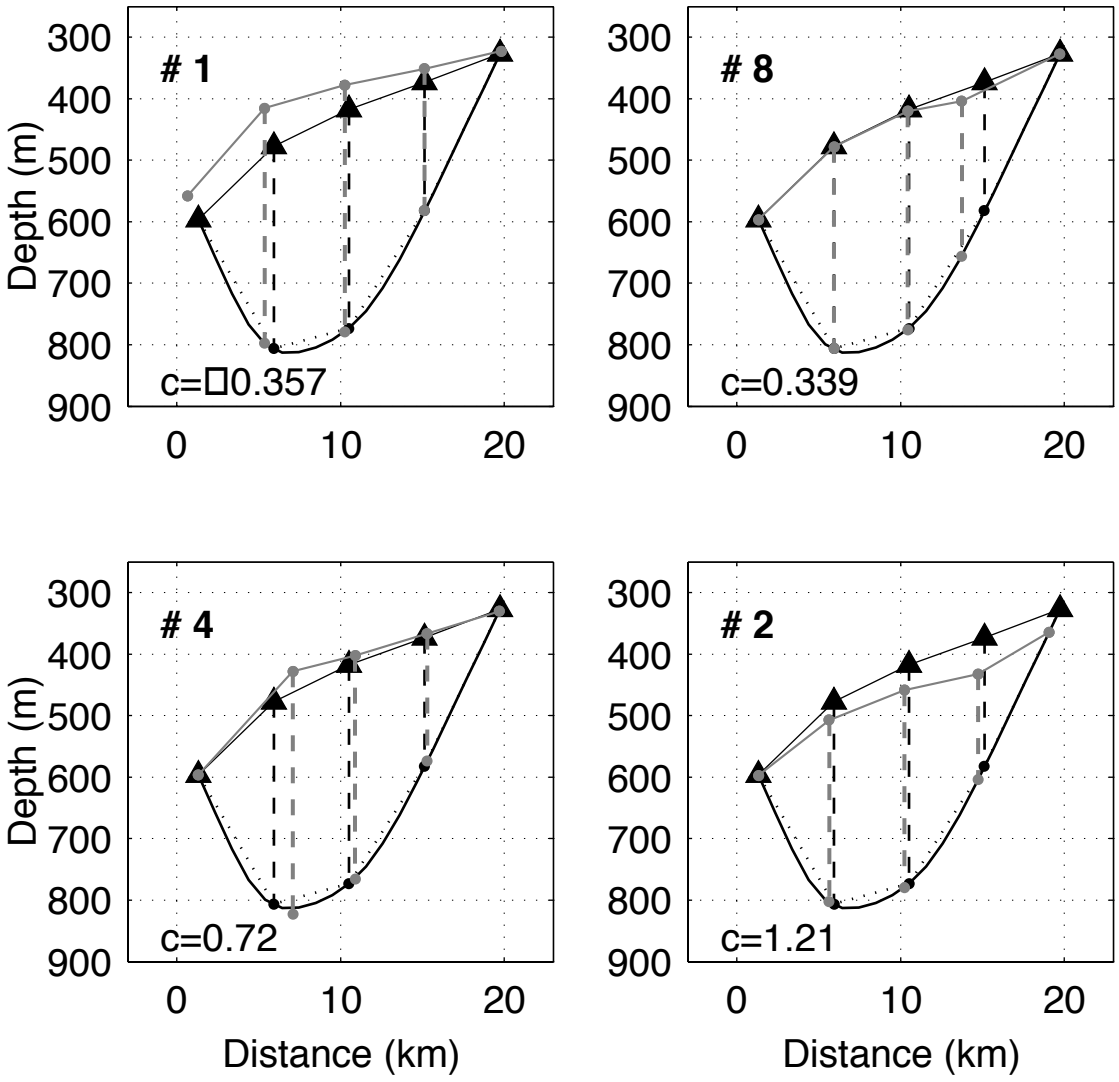

Figure 2.11.13

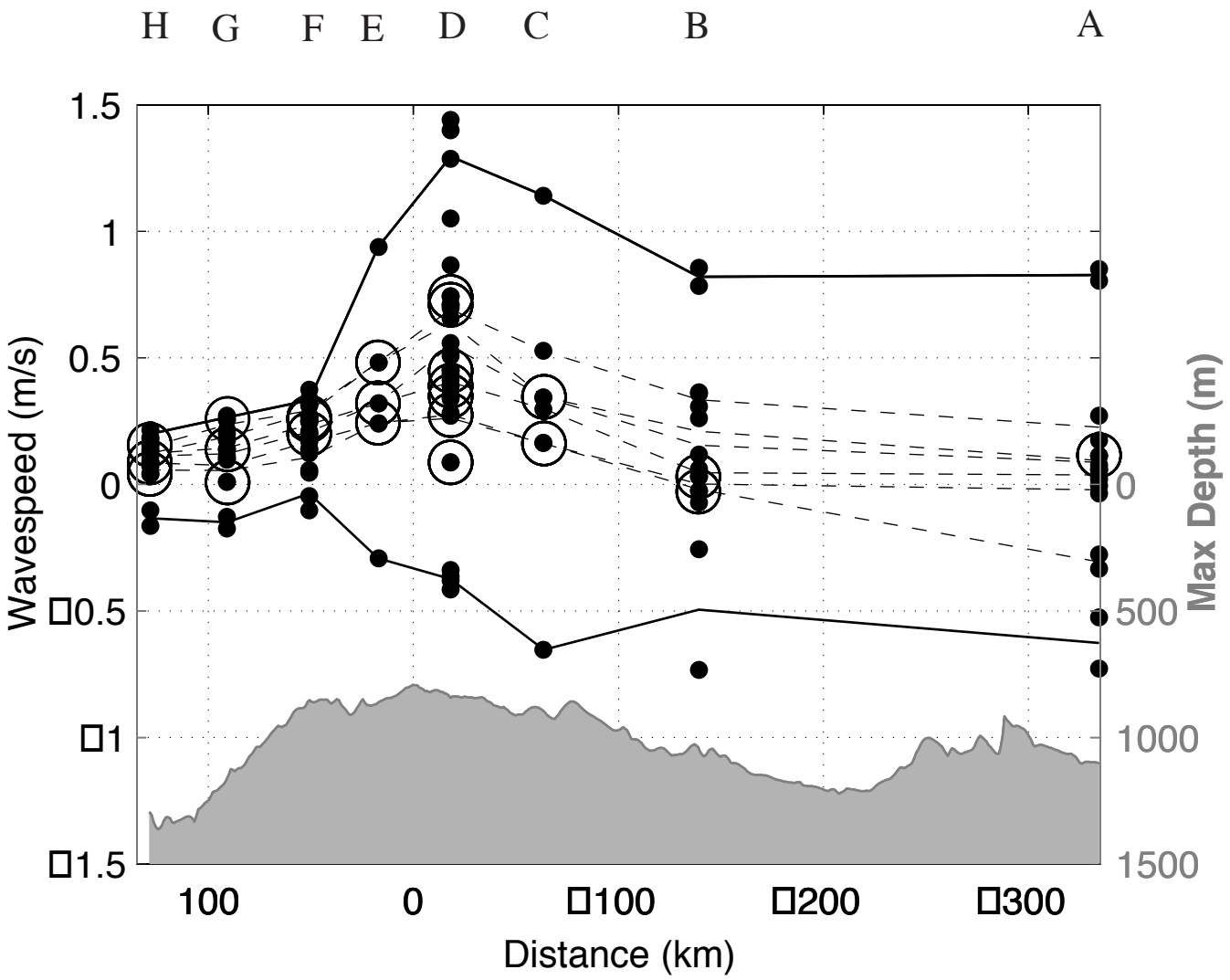

Figure 2.11.14

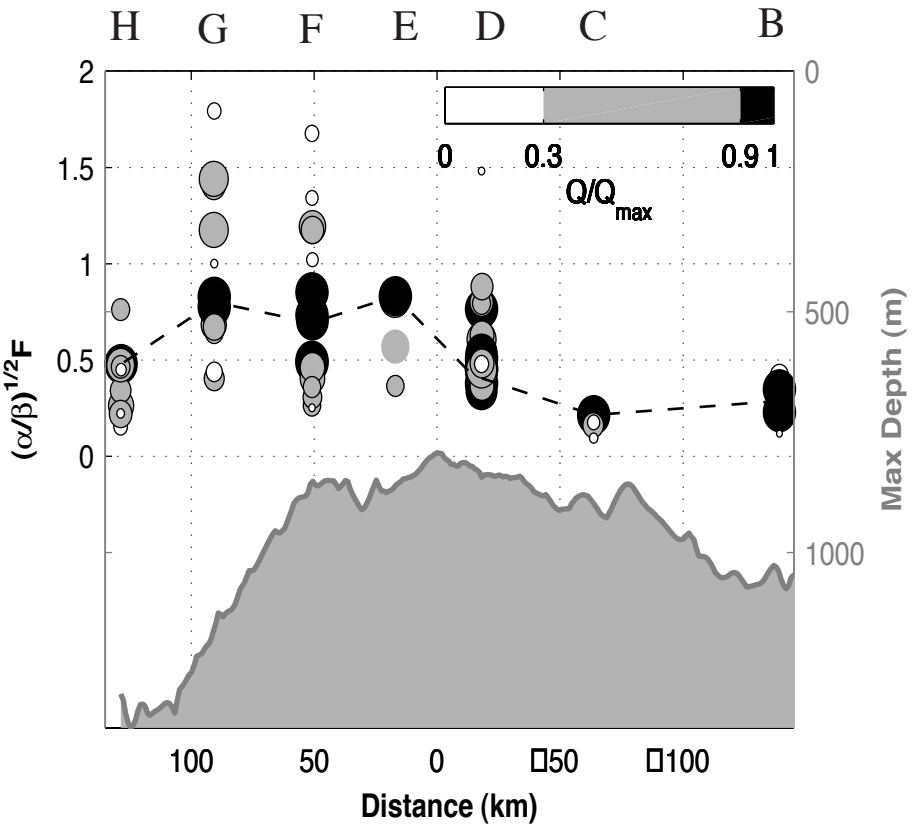

Figure 2.11.15.
adjusted Froude numbers

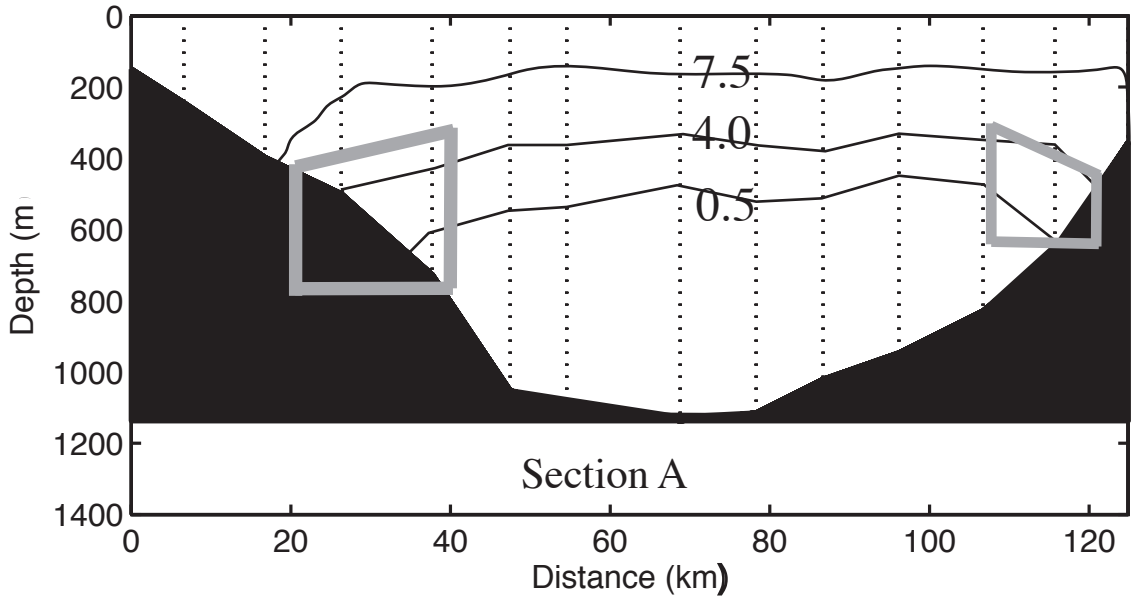

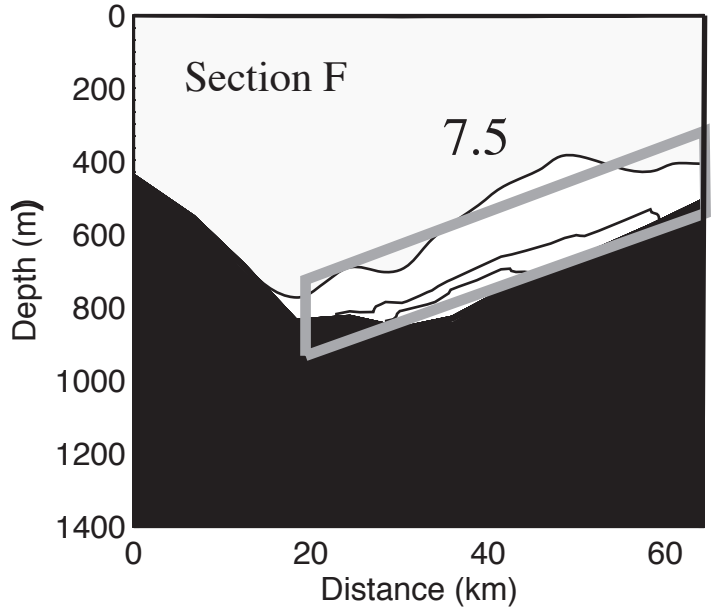

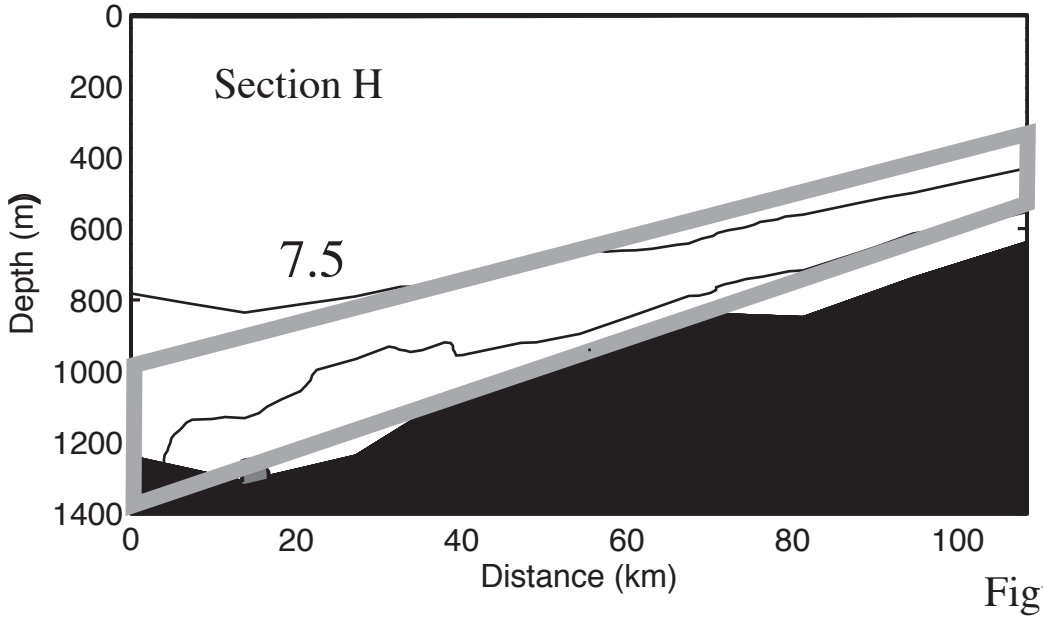

Figure 2.11.16